DOI: 10.26599/FSHW.2026.9251236

Contents lists available at SciOpen

Food Science and Human Wellness

journal homepage: https://www.sciopen.com/journal/2097-0765

China Food Publishing Co.

Protocatechualdehyde from *Taraxacum officinale* Acted as A Competitive Substrate to Inhibit Xanthine Oxidase Attenuates Hyperuricemia

Mingming Li[a,b], Mintong Tian[a,b], Yongzhi Han[a,b], Ce Liu[a,b], Jun Wu[a], Yuan Rao[a,b], Yulong Li[a,b], Xin Yu[a], Jia Wang[a,b], Xinxiao Sun[a,b], Kang Xu[a,b,*], Qipeng Yuan[a,b,*]

[a] *State Key Laboratory of Chemical Resource Engineering, Beijing University of Chemical Technology, Beijing 100029, PR China*

[b] *College of Life Science and Technology, Beijing University of Chemical Technology, Beijing 100029, PR China*

ABSTRACT: The escalating prevalence of hyperuricemia (HUA) poses a formidable challenge to global public health. As the key rate-limiting enzyme in uric acid (UA) biosynthesis, xanthine oxidase (XOD) remains the primary target for therapeutic intervention. However, the inherent toxicity and adverse effects of existing pharmacotherapies necessitate the exploration of safe, natural alternatives. We identified and isolated protocatechuic aldehyde (PCA) as a highly potent XOD inhibitor (IC_{50}=0.250 mM) from *Taraxacum officinale* (TO). It significantly outperforming established natural flavonoids. Mechanistically, PCA uniquely functions as a "slow-turnover substrate" via its C1-aldehyde group. This high-affinity binding coupled (K_m =14 μM) with a slow catalytic turnover (K_{cat}=0.014 s^{-1}) created a "kinetic trap". As a result, XOD tied up in PCA processing for a long period and thus continuously blocking xanthine oxidation. Furthermore, PCA was enzymatically oxidized into protocatechuic acid that a safe and bioactive metabolite, which strictly distinguishes it from clinical drugs like allopurinol that generate toxic intermediates. Furthermore, the aldehyde group was a key group for PCA to exert this mechanism. When the aldehyde group was substituted, PCA loses its function as an XOD substrate, and its XOD inhibition activity decreases by 12.35-fold. Subsequent *in vivo* studies validated the attenuates HUA efficacy of PCA, demonstrating that PCA intervention significantly suppressed XOD activity and reduced UA level in HUA mice. Consequently, PCA restored the disrupted oxidative stress-inflammatory homeostasis and ameliorated HUA-induced renal pathological damage. Overall, our work provided strong scientific evidence supporting TO as a safe and effective dietary supplement or intervention for managing HUA, thereby helping to address the related public health challenges.

Key words: Hyperuricemia; Xanthine Oxidase; *Taraxacum officinale;* Protocatechualdehyde; Uric acid

1. Introduction

Hyperuricemia (HUA) is a metabolic disorder characterized by elevated serum uric acid (UA) level. The prevalence ranges from 2.6% to 36% in different countries and regions[1]. Excessive accumulation of UA is a key factor leading to gout [2]. Furthermore, HUA is also linked to the development and progression of systemic metabolic diseases, including hypertension, chronic kidney disease, and cardiovascular diseases [3]. The global prevalence of HUA is gradually increasing with changes in living standards and dietary structure,

***Corresponding author**
2025500011@buct.edu.cn; yuanqp@buct.edu.cn

Received 3 March 2026
Received in revised from 13 April 2026
Accepted 23 June 2026

which has become a challenge to public health [4]. Therefore, maintaining UA homeostasis to alleviate HUA is of critical importance to public health.

Xanthine oxidase (XOD) is the rate-limiting enzyme in purine catabolism, orchestrating the final two sequential steps of UA production: the oxidation of hypoxanthine to xanthine and, subsequently, of xanthine to UA [5]. Consequently, XOD has been unequivocally established as a critical therapeutic target for modulating UA homeostasis and mitigating HUA. Currently, allopurinol (AP) serves as the first-line clinical XOD inhibitors [1]. AP inhibited XOD as a mechanism-based competitive substrate, its bioconversion yields toxic oxprenolol, driving the search for safe plant-derived alternatives [6-9]. XOD catalyzed the transfer of an oxygen atom from water to aldehydes, which was highly analogous to the enzymatic oxidation of AP into oxprenolol [10]. Consequently, naturally occurring aldehydes possess the inherent potential to act as competitive inhibition substrates for XOD. However, while the XOD-inhibitory activities of several natural aldehydes (e.g., cinnamaldehyde and p-coumaric aldehyde) have been documented, it remains unelucidated whether the aldehyde moiety itself serves as the critical functional determinant driving the inhibition [11,12].

Taraxacum officinale (TO), a perennial herbaceous plant belonging to the Asteraceae family, is widely distributed globally and is well-established as a nutritious food source [13,14]. It has been classified as "Generally Recognized as Safe" by the U.S. Food and Drug Administration and is commonly incorporated into food products such as salads, teas, and coffee substitutes [15]. This history of safe consumption provides a strong foundation for utilizing TO as a functional dietary ingredient for health maintenance. TO contains a rich variety of natural compounds, such as flavonoids and polyphenols. This laid the foundation for the management of HUA as a functional food with metabolic regulatory functions. However, despite its widespread culinary use, systematic scientific evidence supporting the efficacy of TO intake in ameliorating HUA remains limited. Current research is sparse, with only a few studies reporting its ability to reduce serum UA level or inhibit XOD activity. Yao, *et al.* [16] discovered that beer possesses the ability to inhibit XOD activity, with the addition of TO to the fermentation substrate. In addition, TO extract also attenuated the elevated serum UA level in rats with CCl_4-induced oxidative kidney injury [17]. These findings provide supportive evidence for the potential of TO to alleviate HUA by targeting XOD. However, the key XOD inhibitor not been fully elucidated. More crucially, it remains unknown whether any specific natural phenolic aldehyde derived from TO can uniquely function as a competitive substrate, mimicking the potent mechanism-based inhibition of AP to exert a profound effect.

The work aims to an XOD inhibition-guided strategy was used to isolate and identify the key bioactive compounds from TO. The isolation process involved sequential use of silica gel, MCI chromatography, and Sephadex LH-20 chromatography, ultimately yielding the most potent XOD inhibitor, protocatechualdehyde (PCA), through preparative HPLC. Additionally, its effectiveness was verified by establishing an HUA mice model. The spectroscopic analysis, mass spectrometry analysis, and molecular simulation were employed to elucidate the interaction mechanism between PCA and XOD. This work shifts from organ level to molecular level analysis, revealing how PCA directly inhibit XOD. Furthermore, our work provided a new perspective

on how to explore the interaction mechanism between natural small molecules and XOD. In addition, our work provided robust scientific evidence for developing TO as a safe and effective dietary supplement or as a dietary intervention for HUA.

2. Materials and methods

2.1 Chemicals and reagents

TO were purchased from Beijing Tongrentang (Beijing, China). XOD and Xanthine was obtained from Beijing Solarbio Science & Technology Co., Ltd (Beijing, China). Potassium oxonate (PO) was purchased from MedChemExpress Co., Ltd (Shanghai, China) Assay kits UA, XOD, creatinine (Cre), blood urea nitrogen (BUN), adenosine deaminase (ADA), glutathione peroxidase (GSH-PX), and superoxide dismutase (SOD) were purchased from Nanjing Jiancheng Institute of Bioengineering (Nanjing, China). The XOD ELISA kit was purchased from Mlbio Co., Ltd. (Shanghai, China).

2.2 Extraction and isolation of compounds from TO

The separation and extraction of compounds from TO was shown in Fig.1 A. Briefly, 10 kg of TO powder was weighed, and mixed with liquid (water, 60%-90% ethanol) in a 100 L extraction tank at a material to liquid ratio of 1:10. Two extractions were carried out at room temperature for 48 h. The two filtrates were concentrated together, concentrated, and dried to obtain the extract of TO. Based on its promising inhibition of XOD activity, the 60% ethanol extract was selected for further isolation using liquid-liquid partitioning. The extract was resuspended in warm water and first partitioned with petroleum ether. The lower aqueous phase was then collected and separately partitioned with ethyl acetate and dichloromethane to obtain the corresponding fractions. Potent XOD inhibitors was concentrated in the ethyl acetate extract, which was applied to silica gel column. Gradient elution was performed, and the collected similar fractions were combined. Similar chromatographic steps were followed for both MCI and Sephadex LH-20. Final isolation was achieved by preparative HPLC, yielding 11 pure compounds.

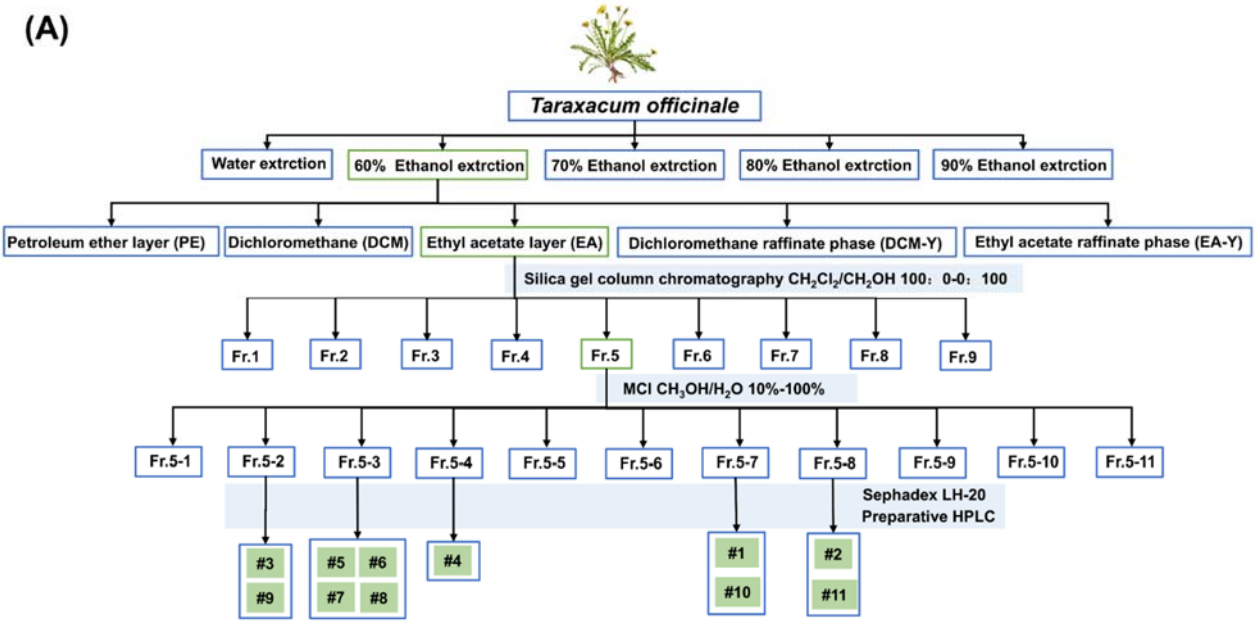

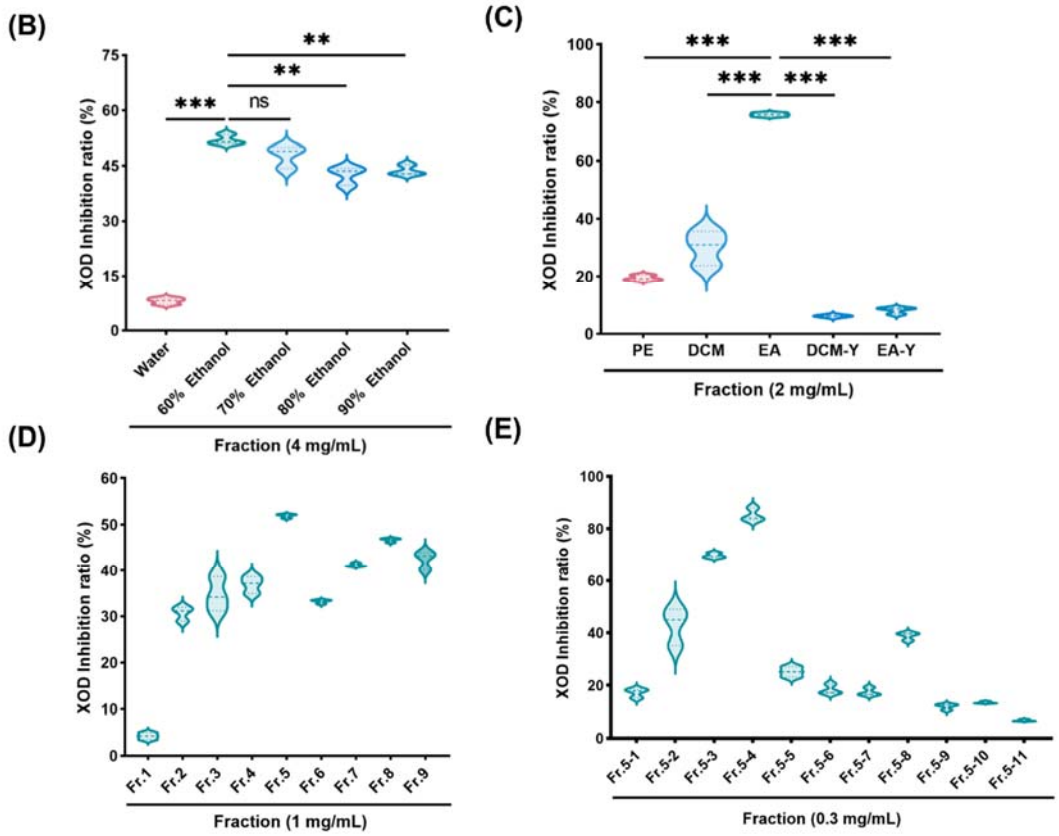

Figure 1. Activity-guided separation based on XOD inhibitory activity. (A) separation procedure; XOD inhibitory activity of (B) different extraction methods, (C) liquid-liquid extracts, (D) fraction from silica gel column chromatography, (E) fraction from MCI column chromatography. ***, P<0.001; **, P<0.01; *, P<0.05.

2.3 Analysis of XOD inhibitory activity

The assay for XOD inhibitory activity was performed with slight modifications to the previously described method [18]. In brief, the mixture solution with 50 μL samples, 50 μL XOD (0.05 U, in 0.01M PBS), and 50 μL xanthine (0.2 mM, in 0.01 M PBS) was incubated. Measurement was performed at 290 nm to monitor the absorbance value of the reaction from the time of enzyme addition, with measurements every 1min for 10 min. The blank group replaced the sample with the same solvent. XOD inhibitory activity was calculated by using the following equation:

$$\text{XOD inhibitory activity } (\%) = \left(1 - \frac{K_{sample}}{K_{blank}}\right) \times 100$$

Where K_{blank} and K_{sample} was the slopes of the regression equation f of the blank group and sample group, respectively.

2.4 Identification of compounds by NMR

For NMR analysis, compounds were respectively dissolved in 600 μL of DMSO-d_6. ^{1}H (600 MHz) and ^{13}C (150 MHz) spectra were recorded on a Bruker AV600 high-resolution NMR spectrometer.

2.5 HUA induction and drug administration

Male C57BL/6J mice (6 weeks old, 20–23 g) were purchased from Charles River Laboratories Co., Ltd. (Beijing, China). The animals were housed in a specific-pathogen-free (SPF) facility under controlled

conditions (25 ± 2 °C, 50 ± 10% humidity, 12 h light/dark cycle) with ad libitum access to standard chow and water. After a one-week acclimatization period, the experimental procedures commenced. All animal protocols were approved by the Institutional Animal Care and Use Committee of Beijing Morningrise Hi-Tech Biotechnology Co., LTD (20250010MSA)

Mice were randomly allocated into five groups (n=6): control, model, PCA-L (50 mg/kg), PCA-H (100 mg/kg), and AP (10 mg/kg) (Fig.7A). To induce HUA, mice in the Model, AP, PCA-L, and PCA-H groups were fed a 0.2% adenine-containing diet an received a daily intraperitoneal (i.p.) injection of PO (250 mg/kg) for 7 days. The dosage (0.2% adenine) ensured that any observed renal impairment is driven by sustained HUA rather than adenine toxicity [19,20]. The control group was fed a standard diet and received i.p. injections of 0.5% sodium carboxymethylcellulose (CMC-Na). Concurrently with model induction, mice were administered their respective treatments by oral gavage once daily for 7 days. PO, PCA, and AP were suspended in 0.5% CMC-Na. The control and Model groups received an equivalent volume of the vehicle (0.5% CMC-Na). On day 1 and 6 of the experiment, all mice were placed in individual metabolic cages for urine collection. One hour after the final administration on day 7, blood was drawn from mice under anesthesia. Then, mice were euthanized via cervical dislocation. Liver and kidney tissues were rapidly excised, rinsed with ice-cold PBS, snap-frozen in liquid nitrogen, and maintained at -80°C until analysis.

2.6 Serum, urine, liver, and kidney-related parameter assays

Serum XOD activity, CRE, BUN, and ADA were measured following the procedures outlined in the respective commercial assay kits. Liver tissue was homogenized in 0.9% saline solution at 10% w/v, centrifuged (4°C, 3000 rpm, 10 min), and the supernatant was collected. The liver XOD activity were measured using a commercial assay kit. The XOD expression level in the liver was quantitatively analyzed using the ELISA kit through the double-antibody sandwich ELISA technique. Subsequently, the ESLIA result was to standardize by measuring the protein content of the homogenized liquid through its organization. Total protein concentration in tissue homogenate supernatant was measured using the BCA protein assay kit Kidney tissue underwent a similar procedure. SOD and GSH-PX activity measurements were performed using commercial kits.

2.7 Kidney IL-1, IL-10 and Kim-1 mRNA expression levels

Following the method described by Han*, et al.* [21], total RNA was extracted from kidney tissue using TRIzol® reagent. The RNA was reverse-transcribed into cDNA according to the manufacturer's instructions. The mRNA levels were determined using SYBR Green real-time PCR Master Mix following the manufacturer's protocol. Table S1 illustrated the primer sequences used in our work.

2.8 Histological analysis

Following fixation in 4% formaldehyde (24 h, room temperature), kidney tissues were embedded in paraffin and sectioned at 5 μm thickness for staining. Tissue morphology and fibrosis were analyzed using

hematoxylin and eosin (H&E) and Masson's trichrome staining, respectively, with images acquired using a light microscope.

2.9 Enzyme kinetic determination

The work employed an inhibition kinetic analysis following previously reported methods with minor modifications [22]. Briefly, PCA (0–0.3 mM) and XOD (0.00125–0.075 U/mL) were mixed, and xanthine (0.0004 M) was added to initiate the reaction. This approach was used to assess the reversibility of enzyme inhibition. XOD (0.05 U/mL) and PCA (0.05–0.3 mM) were mixed, followed by the addition of xanthine (0.00025–0.00075 M) to initiate the reaction. Lineweaver-Burk plots were employed to determine the type of inhibition of PCA [23].

$$\frac{1}{v} = \frac{K_m^{app}}{V_{max}}\left(1 + \frac{[I]}{K_i}\right)\frac{1}{[S]} + \frac{1}{V_{max}}\left(1 + \frac{[I]}{\alpha K_i}\right)$$

$$Sloop = \frac{K_m^{app}}{V_{max}} + \frac{K_m^{app}[I]}{V_{max}K_i}$$

$$Y_{intercept} = \frac{1}{V_{max}}\left(1 + \frac{[I]}{\alpha K_i}\right)$$

Where V and Vmax represented the reaction rate and maximum reaction rate, respectively; K_m^{app}, Ki denoted the apparent Michaelis constant, an inhibition constant, respectively; α is the apparent coefficient; [S] represented the xanthine concentration; [I] denoted the PCA concentration.

2.10 ITC characterized the kinetic parameters of XOD and PCA

The enzymatic kinetic parameters of XOD and PCA as characterized by ITC were determined according to the method reported by Zambelli [24]. Enzyme kinetics (K_m, and k_{cat}) were analyzed at 25 °C using a VP-ITC (MicroCal, Malvern, US) calorimeter. Heat flows from substrate titrations (0–0.08 mM) were directly fitted to the Michaelis-Menten equation.

$$\Delta H = \frac{Q_{total}}{[S]V}$$

$$v = \frac{1}{V}\frac{dQ}{\Delta H}\frac{dt}{} = \frac{K_{cat}\ [E][S]}{K_m + [S]}$$

Where ΔH, Qtotal, [S] and V represented the enthalpy change of the reaction, total cumulative heat, substrate concentration, and the volume of the reaction chamber, respectively; v and dQ/dt denoted the instantaneous rate of the enzymatic reaction and instantaneous thermal power signal, respectively; K_{cat} was the turnover number; K_m represented the Michaelis constant; [E] denoted the enzyme concentration.

2.11 Computational Simulation Analysis

2.11.1 Molecular docking

Molecular docking was performed using Discovery Studio 2019 (Dassault Systems, San Diego, CA, USA). The crystal structure of bovine XOD complexed with quercetin (PDB ID: 3NVY) was obtained from

the Protein Data Bank (https://www.rcsb.org/). The protein structure was prepared by removing water molecules and the co-crystallized ligand, followed by the addition of hydrogen atoms. The continuous enzymatic kinetics results of ITC indicated that PCA can enter the active site of XOD as a substrate. Therefore, the binding site was identified as the catalytic active site of XOD. According to a report by Yu*, et al.* [25], the active site was defined as a 16.5 Å radius sphere centered on the coordinates X: 87.70, Y: 7.70, and Z: 15.97. PCA structure obtained from PubChem (https://pubchem.ncbi.nlm.nih.gov/). PCA were prepared and energy-minimized using the "Prepare Ligands" module. The CDOCKER protocol was then used for the docking simulation. Specifically, 10 random ligand conformations were generated as initial poses, subjected to high-temperature molecular dynamics simulation (700 K, 2000 steps) to overcome local energy barriers, and subsequently cooled through a simulated annealing (5000 steps) to identify energetically favorable binding modes. Final poses were further refined by in-situ energy minimization (5000 steps). The top 10 binding conformations were retained and ranked according to their CDOCKER interaction energy values. The optimal binding pose for each compound was selected based on the lowest -CDOCKER Energy score for further analysis.

2.11.2 Molecular dynamics (MD) simulations

The MD analysis referenced previous reports and made minor modifications[22]. MD simulations were performed using the GROMACS 2022.6 software package. The AMBER99SB-ILDN force field was applied to the protein–ligand system. The system was solvated in a cubic box with a 1.0 nm minimum distance between the protein and the box boundaries, using the TIP3P water model, and ion concentration was neutralized with counterions. Energy minimization was carried out using the steepest descent algorithm until the maximum force fell below 1000 kJ/(mol·nm). Subsequently, the system was equilibrated under the NVT ensemble for 2 ns, followed by equilibration under the NPT ensemble for 1 ns at 298.15 K and 1 bar. Finally, a production MD simulation was conducted for 100 ns under the same temperature and pressure conditions. After simulation, trajectory analyses including root- RMSD, SASA, RMSF and Rg were performed to evaluate the dynamic behavior and binding stability between XOD and PCA.

2.12 Conversion of PCA by XOD

A total of 500 μL XOD (1 U/mL) was mixed with 500 μL sample (0.2 mM). Then, the reaction mixture was incubated at room temperature for 12 h in the dark. The resulting solution was subjected to HPLC and LC-MS analysis. In this work, the following groups were established: PCA-XOD, PCA, XOD, and PCA-heat inactivated XOD (PCA-HKXOD). XOD was replaced with a solvent in the PCA group, while PCA was replaced with a solvent in the XOD group. Xanthine is not present in any of the groups. HPLC analysis was performed on a Shimadzu LC-20AT system equipped with an SPD-M20A DAD detector. Separation was achieved using a C18 column (250 × 4.6 mm, 5 μm; NanoChrom Technologies). The mobile phase consisted of (A) water with 0.02% trifluoroacetic acid (TFA) and (B) methanol. A linear gradient of 10–60% B was applied over 25 min at a flow rate of 0.9 mL/min. The column temperature was maintained at 40 °C, and the

injection volume was 10 μL. Detection was carried out at 254 nm. The LC-MS analysis was conducted following the method proposed by Tian*, et al.* [26].

2.12 Statistical analysis

Data analysis and graphing were performed using GraphPad and Origin software. Data are presented as mean ± standard error of the mean (SEM). The t-tests were performed to assess statistical significance. The test results were considered statistically significant at $*P < 0.05$, $**P < 0.01$, and $***P < 0.001$.

3. Results

3.1 Inhibiting XOD activity-Guided Isolation

Solvents with varying polarities demonstrate distinct efficiencies in enriching the target active compound. The XOD inhibitory activity of extracts prepared using water and 60%-90% ethanol has been assessed. The results revealed that the 60% ethanol extract exhibited superior inhibitory activity (Fig.1B). Hence, the 60% ethanol was therefore selected for subsequent liquid-liquid partition. The EA fraction showed notably high XOD inhibitory activity (Fig.1C). Based on this finding, the EA fraction was further separated by silica gel column chromatography with a gradient elution of dichloromethane/methanol (0-100%). Among the collected fractions (Fr.1-Fr.10), the Fr.5 displayed the most potent XOD inhibitory effect (Fig.1D). Consequently, the Fr.5 was subjected to MCI column chromatography for the isolation of key bioactive compounds. The subfractions from MCI column chromatography exhibiting XOD inhibitory activity (Fig.1E) and suitable polarity were purified through repeated gel filtration chromatography on Sephadex LH-20, followed by preparative high-performance liquid chromatography, yielding 11 pure compounds.

3.2 Compounds isolated from TO

TO contains abundant natural compounds including polyphenol, alkaloid, and sesquiterpene [14]. Among they, polyphenol have been extensively studied for their inhibitory effects XOD [6,27]. The Fig.2 illustrates the isolation of 11 compounds from TO in our work, including polyphenol (8), coumarin (1), sesquiterpene (1), and others (1). ^{1}HNMR and ^{13}C NMR spectra of 11 compounds were shown in Fig.S1-Fig.S11. These findings align with the established phytochemical profile of TO. Among these compounds, such as luteolin, esculetin, and p-coumaric acid, their ability to inhibit XOD and alleviate hyperuricemia has been demonstrated both in vivo and in vitro. [28-31]. Notably, the XOD inhibitory activity of 1# (6-Hydroxy-4-methoxyquinolin-2(1H)-one), 5# (1β,3β,6α-Trihydroxy-4α(15)-dihydro-magnol-18-en-20-oic acid methyl ester), and 6# (PCA) the relevant information is limited. Thus, in order to screen for the most potent XOD inhibitor, the inhibitory activity of these compounds will be further assessed and compared against established inhibitors like luteolin.

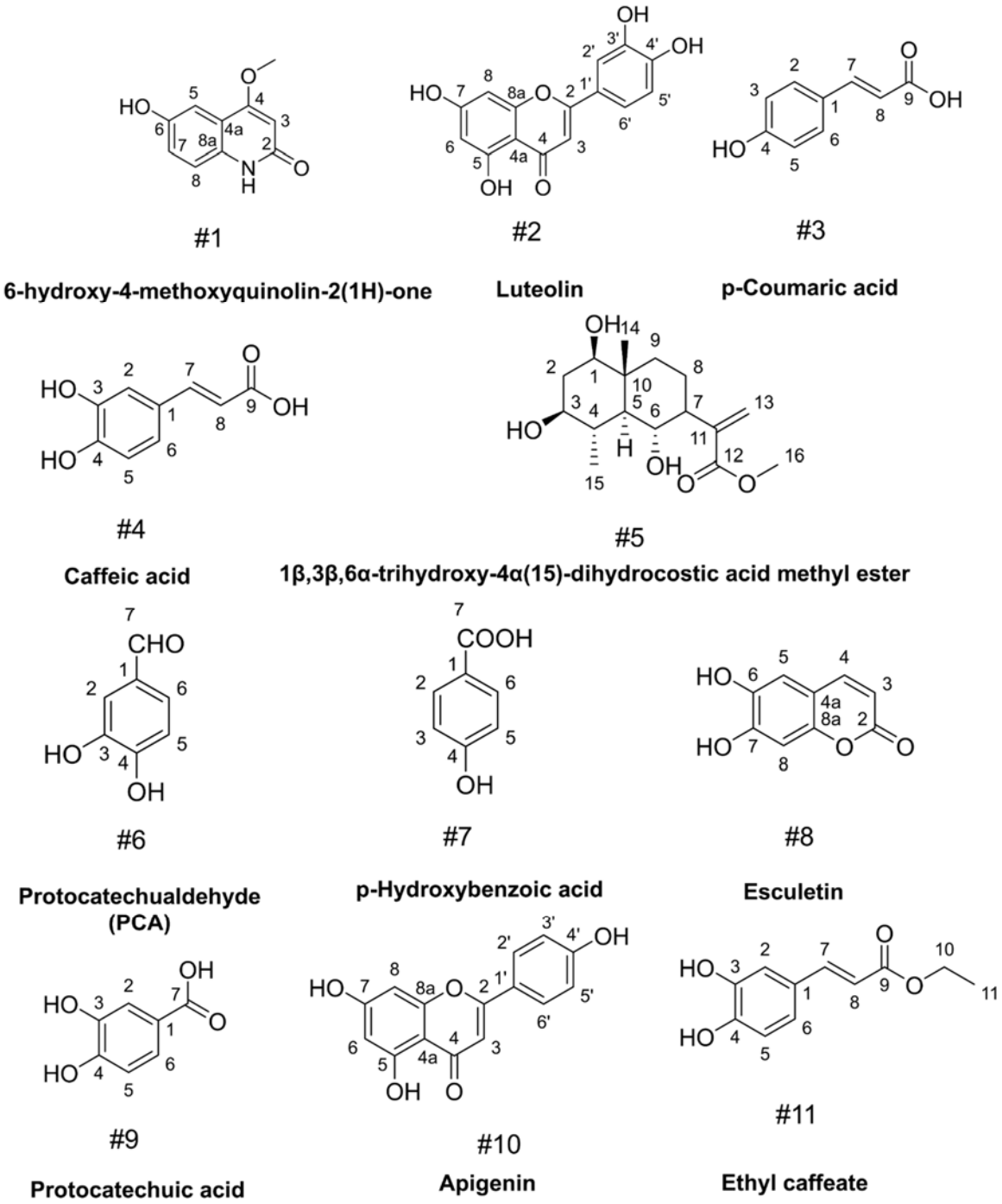

Figure 2. The structures of 11 compounds isolated from TO

3.3 PCA was the most potent inhibitor of XOD

To screen for potent XOD inhibitors, the inhibitory XOD activity of 11 key compounds was evaluated. When the concentration of inhibitors reached 1.0 mM, the XOD inhibition rate of caffeic acid and PCA reached 98.40% and 93.05% (Fig.3A), respectively. The XOD inhibition rate (>50% from 1 mM) of other compounds was as follows: *p*-coumaric acid > luteolin > ethyl caffeate > apigenin (Fig.3A). Furthermore, after standardizing the concentration units of the individual compounds and their corresponding crude extracts, all six compounds (< 0.3 mg/mL) showed significantly higher XOD inhibitory activity than the crude extracts (0.3 mg/mL) (Fig.S12). That suggested that the activity of the crude extracts was attributable to these

active monomers. Based on these results, these compounds were selected for IC_{50} determination to further characterize their XOD inhibitory effects. As shown in Figure 3B-H, PCA exhibited potent XOD inhibitory activity with an IC_{50} value (0.250 mM) lower than other compounds, surpassing established natural XOD inhibitors, such as caffeic acid, luteolin, apigenin, and p-coumaric acid. Therefore, as the most potent inhibitor derived from TO, PCA was selected for in-depth investigation to explore the molecular mechanism of inhibition XOD activity and its *in vivo* efficacy.

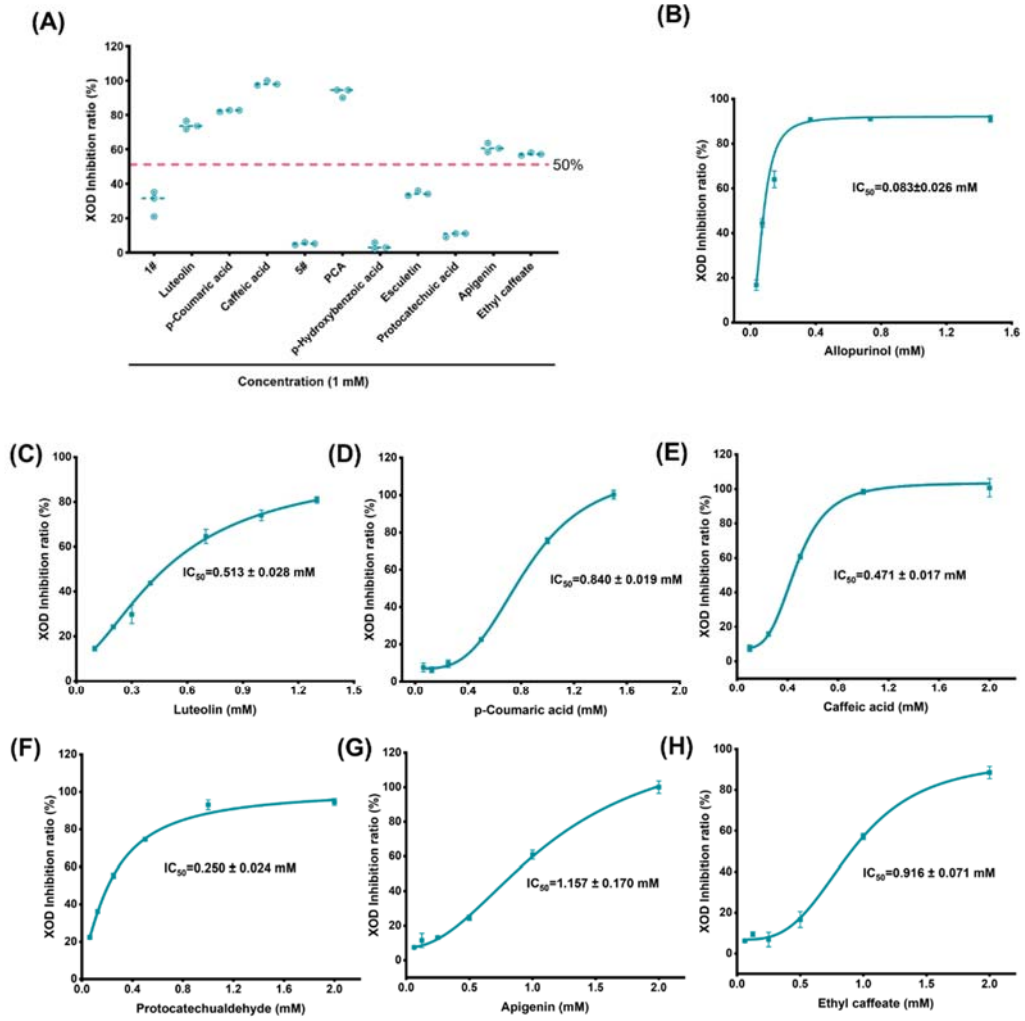

Figure 3. XOD inhibitory activity of the 11 isolated compounds. (A) The XOD inhibitory activity of different compounds (1 mM); The IC_{50} value of (B) AP, (C) Luteolin, (D) p-Coumaric acid, (E) Caffeic acid, (F) PCA, (G) Apigenin, and (H) Ethyl caffeate.

3.4 PCA decreased UA level by inhibiting XOD activity

To further validate the function by which PCA alleviates HUA by inhibiting XOD activity and reducing UA production, a HUA mouse model was established (Fig.4A). Similar to *in vitro* experiments, serum XOD activity was inhibited by PCA in HUA mice (Fig.4C). The liver is postulated to be the primary source of circulating XOD [32]. Hence, XOD activity and expression were quantified in liver tissue. The Fig.4D illustrated that XOD activity in the liver was also regulated by PCA, restoring it to level comparable to the normal group. Similarly, a comparable phenomenon was observed in liver XOD expression levels, which decreased by 32.2%. Moreover, the effect was superior to that of AP (Fig.4E). That result in reduced UA

synthesis and maintain UA homeostasis in HUA mice by directing XOD. Compared to the control group, serum UA of HUA mice significantly raised to 1.95-fold, which was decreased 34.3 % by PCA (100 mg/kg) administration (Fig.4F). A similar phenomenon was observed in urine UA. Administration of PCA reduced urine UA to a level comparable to the control group, demonstrating comparable efficacy to the positive control drug AP (Fig.4G). This indicated that the reduction in the body's UA levels was achieved by blocking the synthesis pathway, rather than by promoting the excretion pathway. Additionally, we focused on adenosine deaminase (ADA), a crucial enzyme in purine metabolism. ADA accumulates precursors for UA biosynthesis. Notably, the ADA activity in the PCA group was reduced by nearly 38.2% compared to the model group (Fig.4H). Unfortunately, AP did not exhibit this function. Collectively, the above findings further supported PCA directly targets the key rate-limiting enzyme in the UA synthesis process, reducing UA synthesis and thereby alleviating HUA.

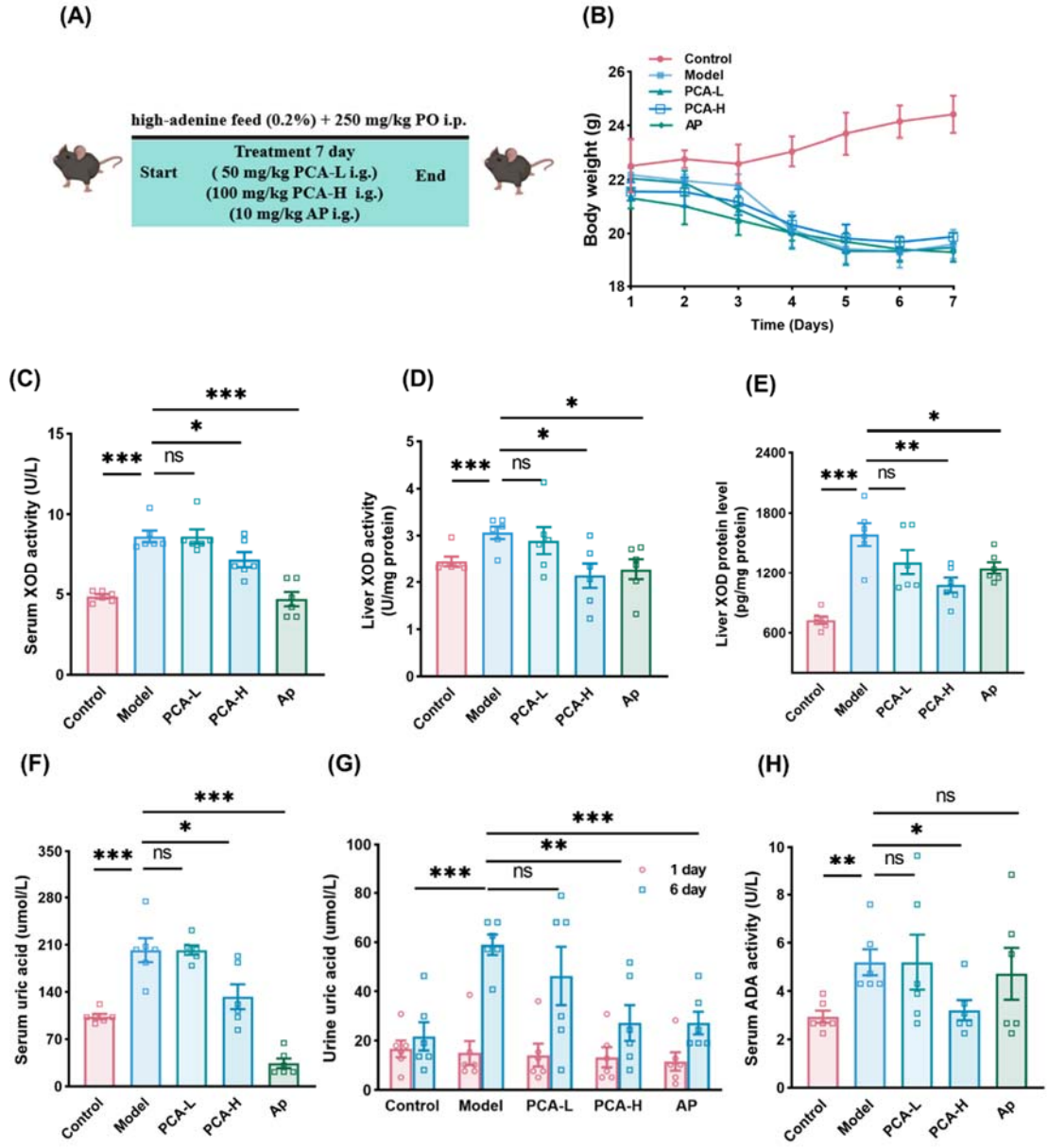

Figure 4. Effects of PCA on HUA Mice. (A) Schematic diagram of the HUA mice with PCA or AP treatment; (B) Changes in body weight; (C) Serum XOD activity; (D) Liver XOD activity; (E) Liver XOD protein level; (F) Serum UA level; (G) Urine UA level; (H) Serum ADA activity. ***, P<0.001; **, P<0.01; *, P<0.05.

3.5 PCA reshaped the kidney oxidative stress-inflammatory microenvironment in HUA mice

In the model group, the high UA burden resulted in a collapse of the antioxidant defense, characterized by decreased (superoxide dismutase) SOD and glutathione peroxidase (GSH-PX) activity, alongside an inflammatory imbalance (elevated IL-1β and reduced IL-10) (Fig.5A-D). Following the PCA intervention, these oxidative stress and inflammatory markers were significantly ameliorated. The activities of SOD and GSH-PX were restored, and the level of IL-1β and IL-10 were rebalanced. These findings suggest that the improvement in the kidney oxidative stress-inflammatory microenvironment was reshaped.

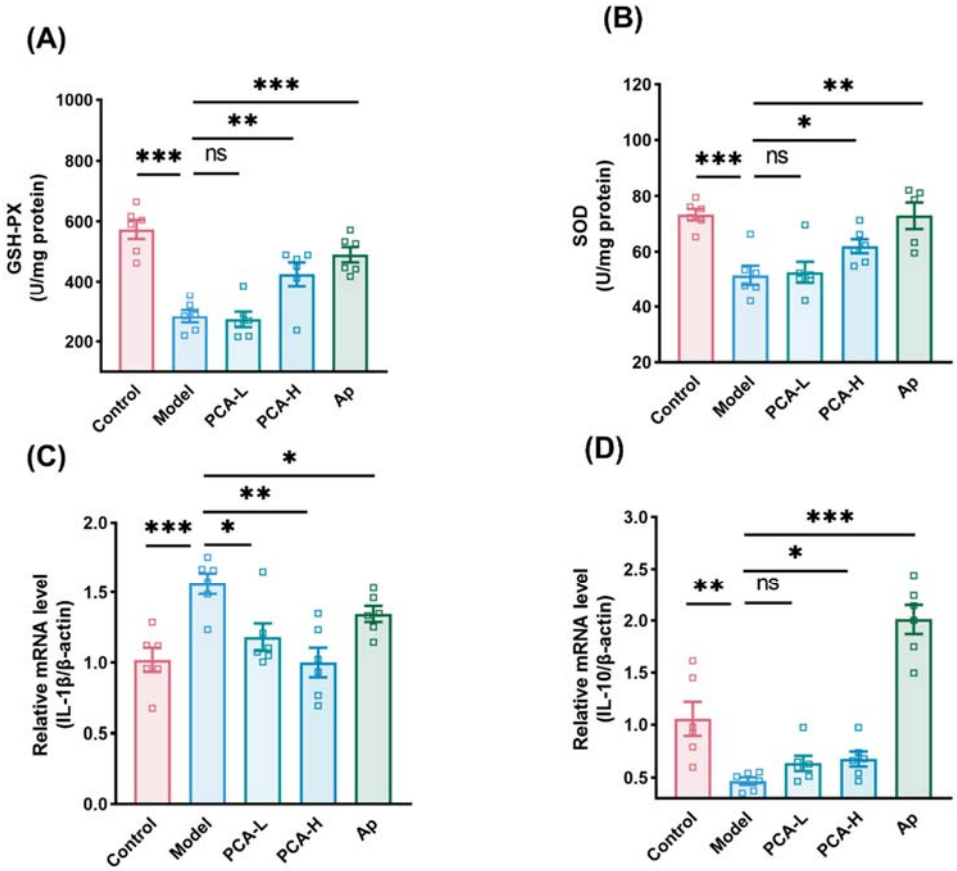

Figure 5. Effects of PCA on the oxidative stress-inflammatory microenvironment in the kidney of HUA mice. (A) GSH-PX activity; (B) SOD activity; (C) IL-1β mRNA level; (D) IL-10 mRNA level. ***, $P<0.001$; **, $P<0.01$; *, $P<0.05$.

3.6 Effect of PCA on kidney functional and pathological injury in HUA mice

Compared with the control group, the level of creatinine (CRE) and blood urea nitrogen (BUN) of HUA mice were increased, suggesting kidney function was damaged in HUA mice. Treatment with PCA reduced the serum CRE and BUN level (Fig.6A, B). Kim-1 is a specific marker of renal tubular injury, which is a direct indicator of kidney damage [33].The Fig.6C demonstrates that PCA treatment reverses the abnormally elevated Kim-1 mRNA level in the kidney of HUA mice. Its efficacy was comparable to that of AP. Histopathological examination was performed to evaluate the structural integrity of the kidneys and the extent of renal injury (Fig.6D, E). The HUA mice displayed severe pathological aberrations indicative of HUA-induced kidney injury. These structural derangements included widespread tubular dilation, vacuolar degeneration of tubular epithelial cells, glomerular distortion, and marked infiltration of inflammatory cells within the kidney interstation. However, PCA treatment markedly attenuated these histopathological

alterations, as evidenced by preserved glomerular architecture, reduced tubular dilation, and diminished inflammatory cell infiltration. In addition, Masson's trichrome staining revealed extensive collagen deposition in the kidney interstation of HUA mice. In contrast, PCA administration markedly reduced this deposition (Fig.6F, G), which revealed that PCA may alleviate kidney fibrosis in HUA mice.

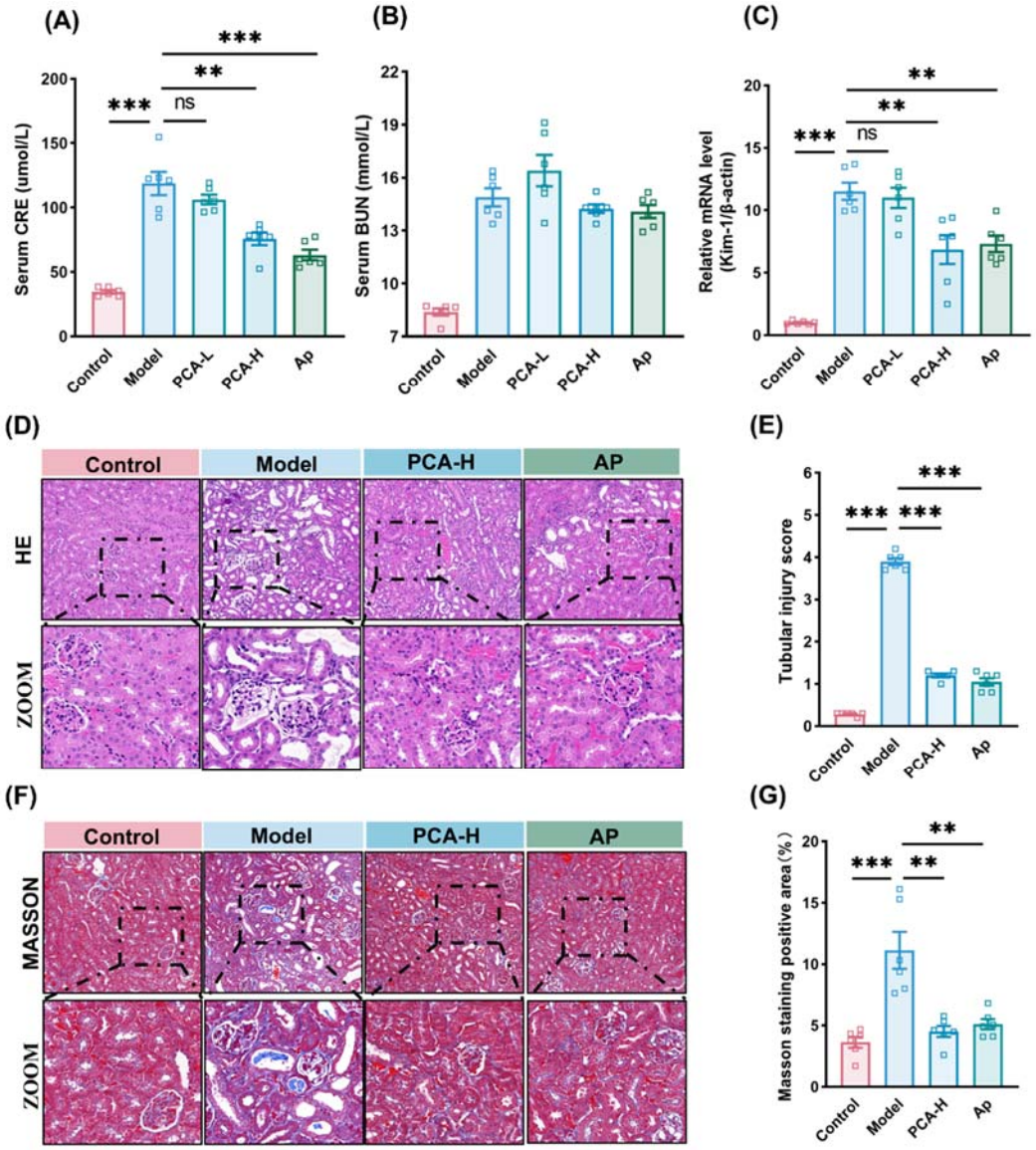

Figure 6. Effects of PCA on kidney function and pathological injury in HUA mice. (A) Serum CRE level; (B) Serum BUN level; (C) Kim-1 mRNA level; (D) H&E staining of kidney; (E) Tubular injury score; (F) Masson staining of kidney; (G) Masson staining positive area. ***, P<0.001; **, P<0.01; *, P<0.05.

3.7 PCA acted as a reversible mixed-type competitive XOD inhibitor

To elucidate the specific interaction mechanism, the work assessed the type of PCA inhibition on XOD by plotting the relationship between ν and [XOD] at different PCA concentrations and performing Lineweaver-Burk plots. As shown in Fig.7A, all lines pass through the origin. In addition, the slope decreased with increasing PCA concentration, which indicated that PCA acts as a reversible XOD inhibitor. Reversible inhibition encompasses competitive, non-competitive, anti-competitive, and mixed inhibition. In Fig.7B, all data lines intersected in the second quadrant of the double reciprocal Lineweaver-Burk plot. Both the X-intercept ($-1/K_m^{app}$) and Y-intercept ($1/V_{max}$) increased with rising PCA concentrations, indicating that PCA

inhibited XOD activity via mixed competitive inhibition. That indicated combination of competitive and non-competitive inhibition. Additionally, the slope and Y-intercept showed linear correlation with PCA concentration (Fig.7C, D), which was suggesting the presence of a single or homologous binding site on XOD [34]. Hydrophobic interactions likely dominate the binding mechanism [35]. In order to further determine which type of inhibition was dominant. We examined the absolute ratio of the X/Y coordinates of the intersection point. As shown in Figure 7E, the absolute value of X/Y was 0.031, which was less than 1. In addition, apparent coefficient α was 5.2. These results indicated that competitive inhibition played a dominant role in PCA's inhibition of XOD activity (X/Y<1, 1<α<10) [23,36,37]. K_m^{app} increased with increasing PCA concentration. This was attributed to the fact that increased inhibitors concentration reduced free enzyme availability via enzyme-inhibitors complex formation, forcing substrate competition and thereby elevating the K_m^{app} [38]. ITC experiments also showed that continuous PCA titration caused persistent heat and baseline drift without returning to the initial baseline (Fig.S13), which was typical of ongoing enzymatic conversion. Enzyme kinetic analysis using continuous ITC gave a typical Michaelis-Menten saturation curve (Fig.7F), with apparent K_m=14 μM, K_{cat}=0.014 s^{-1}, and ΔH=−16 kcal/mol. Thus, in a process dominated by competitive inhibition, PCA primarily acted as a competitive substrate by binding to the catalytic active site of XOD.

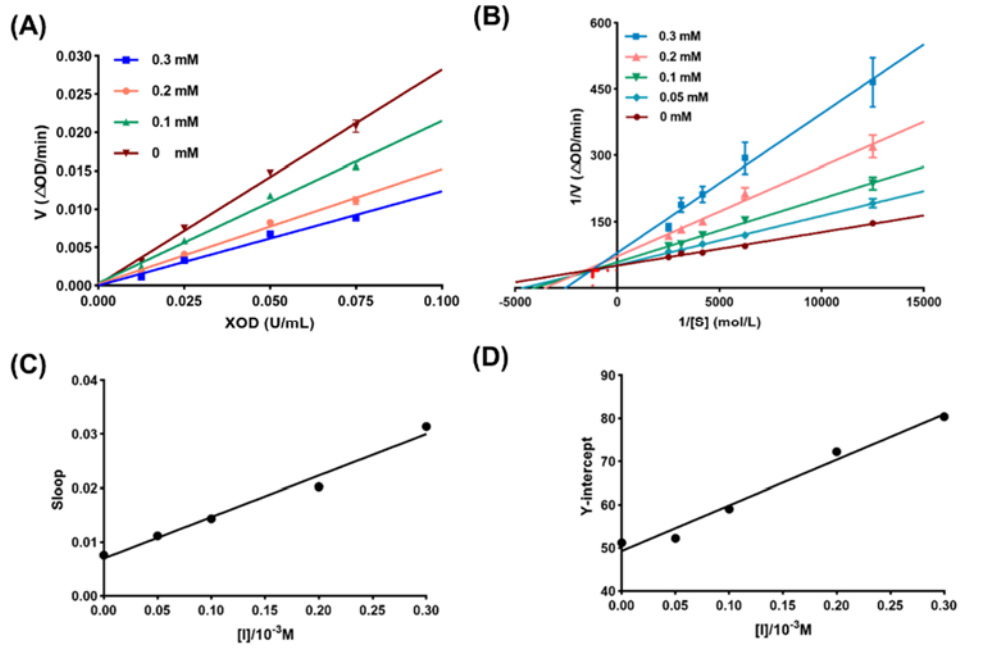

(E)

Inhibition kinetics parameters and types of PCA to XOD from Lineweaver-Burk plots

Concentration / mM	K_i	X/Y	α	K_m^{app}	V_{max}	Inhibition types
0				0.1478	0.0195	
0.05				0.2137	0.0191	
0.1	0.0954	0.031	5.2	0.2432	0.0169	Mixed inhibition
0.2				0.2804	0.0138	
0.3				0.3908	0.0124	

(F)

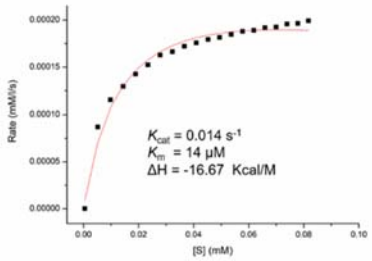

Figure 7. The inhibitory mechanism of PCA on XOD. (A) Plots of ν vs [XOD]. c(PCA) = 0, 0.1, 0.2, 0.3 mM; (B) Lineweaver–Burk plots. c(PCA) = 0, 0.05, 0.1, 0.2, 0.3 mM for curves; (C, D) The secondary plot meant Slope and Y-intercept vs [PCA], respectively. (E) Inhibition kinetics parameters and types of PCA to XOD from Lineweaver-Burk plots. (F) Enzymatic kinetic parameters of XOD and PCA

3.8 Molecular docking and MD simulation analysis

To elucidate the interaction between PCA and XOD, molecular docking was performed. As illustrated in Fig. 8A, PCA docks into the active site of XOD, thereby obstructing substrate access. The calculated -CDOCKER_ENERGY and -CDOCKER_INTERCTION_ENERGY for this pose were 30.0255 kcal/mol and 30.119 kcal/mol. The active site of XOD comprises 18 amino acids, of which Glu802, Arg880, Phe914, Phe1009, and Glu1261 are directly involved in catalysis [3]. The binding pose of PCA shows its insertion into the XOD active site, where specific hydrogen bonds were formed with Glu802 (via the C-4' hydroxyl) and Arg880 (via the aldehyde group). Stabilizing interactions (π−π effects and hydrogen bond) with proximal residues (Phe914, Phe1009, Thr1010) further secure PCA in the binding pocket, thereby facilitating its own binding while obstructing xanthine access. Collectively, these results confirm a competitive inhibition mechanism, consistent with the kinetic data.

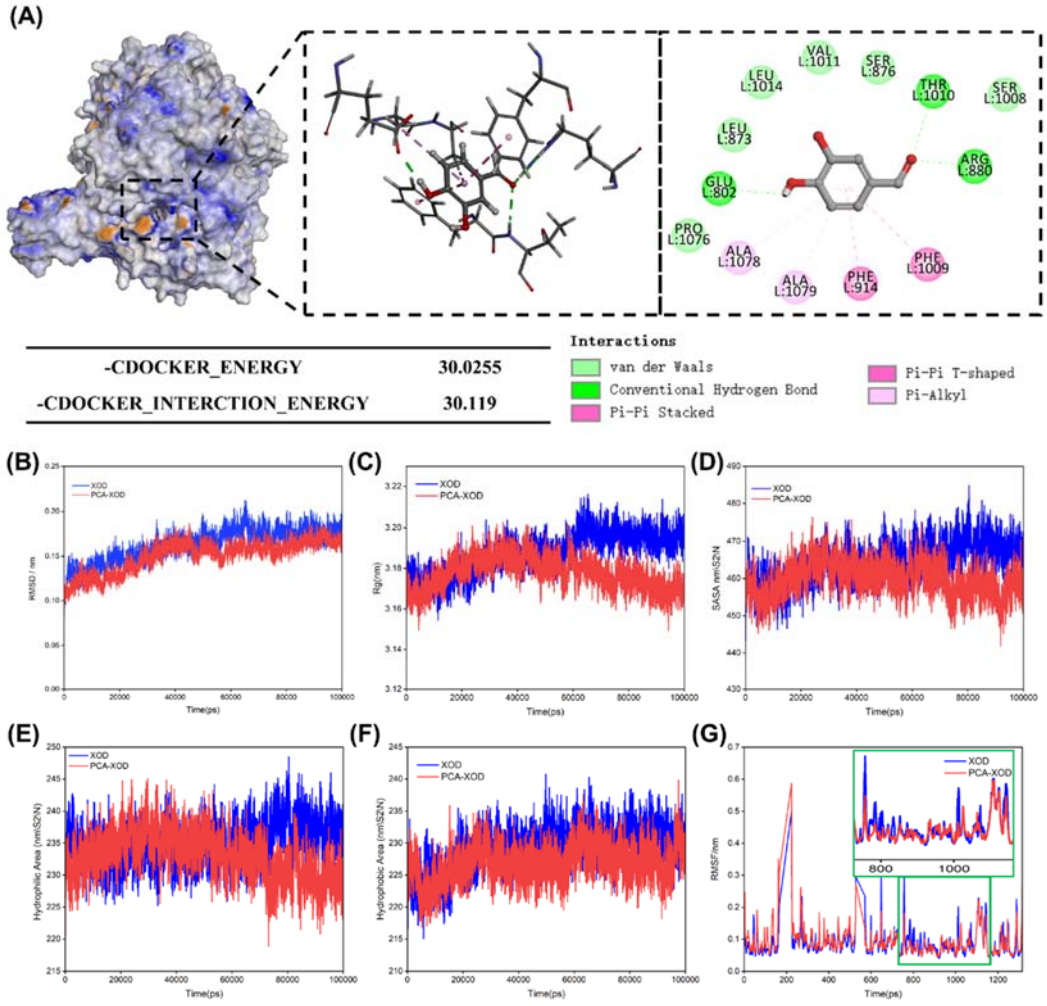

Figure 8. Molecular docking and MD simulation analysis of PCA-XOD system. (A) Molecular docking; (B) RMSD values; (C) Rg values; (D) SASA values; (E) Hydrophilic area; (F) Hydrophobic area; (G) RMSF values.

To elucidate the conformational dynamics and stabilization mechanism of XOD upon binding with PCA, a 100 ns MD simulation was conducted. Analysis of the backbone RMSD revealed that the PCA-XOD complex achieved equilibrium (40 ns) at a significantly lower value (0.16 nm) than the XOD (0.18 nm), indicating that PCA binding markedly enhances overall structural stability (Fig.8B). This enhanced stability

was corroborated by the radius of Rg, where the PCA-XOD complex maintained a consistently lower Rg value, signifying a more compact protein conformation the simulation (Fig.8C). The mechanistic basis for this stabilization was elucidated by the SASA analysis. The observed reduction in total SASA (Fig.8D) was predominantly attributed to a significant decrease in the hydrophobic SASA (Fig.8F), while the hydrophilic SASA remained largely unchanged (Fig.8E). This highlights that the burial of hydrophobic residues from the solvent is a primary thermodynamic driving force for complex formation and stabilization. Finally, analysis of the RMSF demonstrated the local impact of PCA binding. Residues within key functional regions of the PCA-XOD complex (e.g., 800-1000) exhibited a pronounced reduction in flexibility compared to the apo-enzyme (Fig.8G). This local rigidification, occurring at or near the active site, further contributes to the stabilization of the catalytically relevant conformation. Collectively, molecular simulations provide evidence that PCA binding stabilizes the XOD structure by inducing a more compact and less flexible state, a process mechanistically driven by both the global burial of hydrophobic surfaces and the local rigidification of key active-site residues.

3.9 The potential mechanism by which PCA inhibits XOD activity

XOD comprises a class of molybdenum-containing enzymes capable of catalyzing the transfer of oxygen atoms from water molecules to substrates (such as xanthine or aldehydes) [39]. Fig.9A, B illustrated the formation of a novel compound within the PCA-XOD reaction system. In contrast, only PCA is present in the PCA and PCA-HKXOD systems. At 12 h, the PCA content in the PCA-XOD, PCA-HKXOD, and PCA systems was 76.0 μM, 98.4 μM, and 98.0 μM, respectively. Additionally, the content of protocatechuic acid in the PCA-XOD system was 14.7 μM. Mass spectrometry analysis further confirmed that XOD catalyzes the oxidation of PCA to yield protocatechuic acid. As shown in Fig.9C, two $[M-H]^-$ were observed in the PCA–XOD system at m/z 137.03503 (corresponding to PCA) and m/z 153.03604 (corresponding to protocatechuic acid). In contrast, only the deprotonated PCA ion $[M-H]^-$ (m/z 137.05304 and m/z 137.05203) was detected in the PCA and PCA–HKXOD systems. In brief, access to the active site enables PCA to interact with key amino acid residues, facilitating its secure anchoring in the catalytic pocket. Then, the conserved glutamate residue (GLU1261) acted as a general base to abstract a proton from the equatorial Mo–OH group. The resulting activated oxyanion performs a nucleophilic attack on the carbonyl carbon of the PCA substrate. Concomitantly, a hydride transfer occurs from the substrate's formyl C–H bond to the terminal sulfide ligand, effectively reducing the metal center from Mo (VI) to Mo (IV) and generating a Mo–SH moiety. This concerted step leads to the formation of a transient covalent intermediate. Subsequent hydrolysis of the Mo–O–C bond releases the product, protocatechuic acid. The catalytic cycle concludes with the reoxidation of Mo (IV) to Mo (VI) by molecular oxygen (Fig.9D). In summary, PCA acts as a competitive substrate that binds to XOD and was oxidized to protocatechuic acid. This process blocks the access of UA substrates (such as xanthine), thereby blocking the enzymatic pathway for UA production. The function of PCA as a competitive substrate was attributed to the aldehyde group at the C-1 position. To validate the role of the aldehyde moiety, we investigated the effect of its substitution with a carboxyl group at C-1 (protocatechuic

acid) on the inhibitory activity against XOD. Further analysis of the protocatechuic acid-XOD system indicated that no new compounds were formed within the protocatechuic acid-XOD system (Fig.9E). This result highlights the critical importance of the C-1 aldehyde group for PCA's function as a competitive substrate, as its substitution leads to the loss of PCA's ability to act as a competitive substrate. Fig.9F, G illustrated the IC_{50} value of protocatechuic acid was 3.087 mM, which was 12.35-fold higher than that of PCA. This indicated that when the PCA loses its capability of acting as a competitive substrate, its ability to block the pathway of UA production was reduced. Overall, PCA inhibits XOD's ability to catalyze substrate conversion into UA by acting as a competitive substrate that binds to XOD.

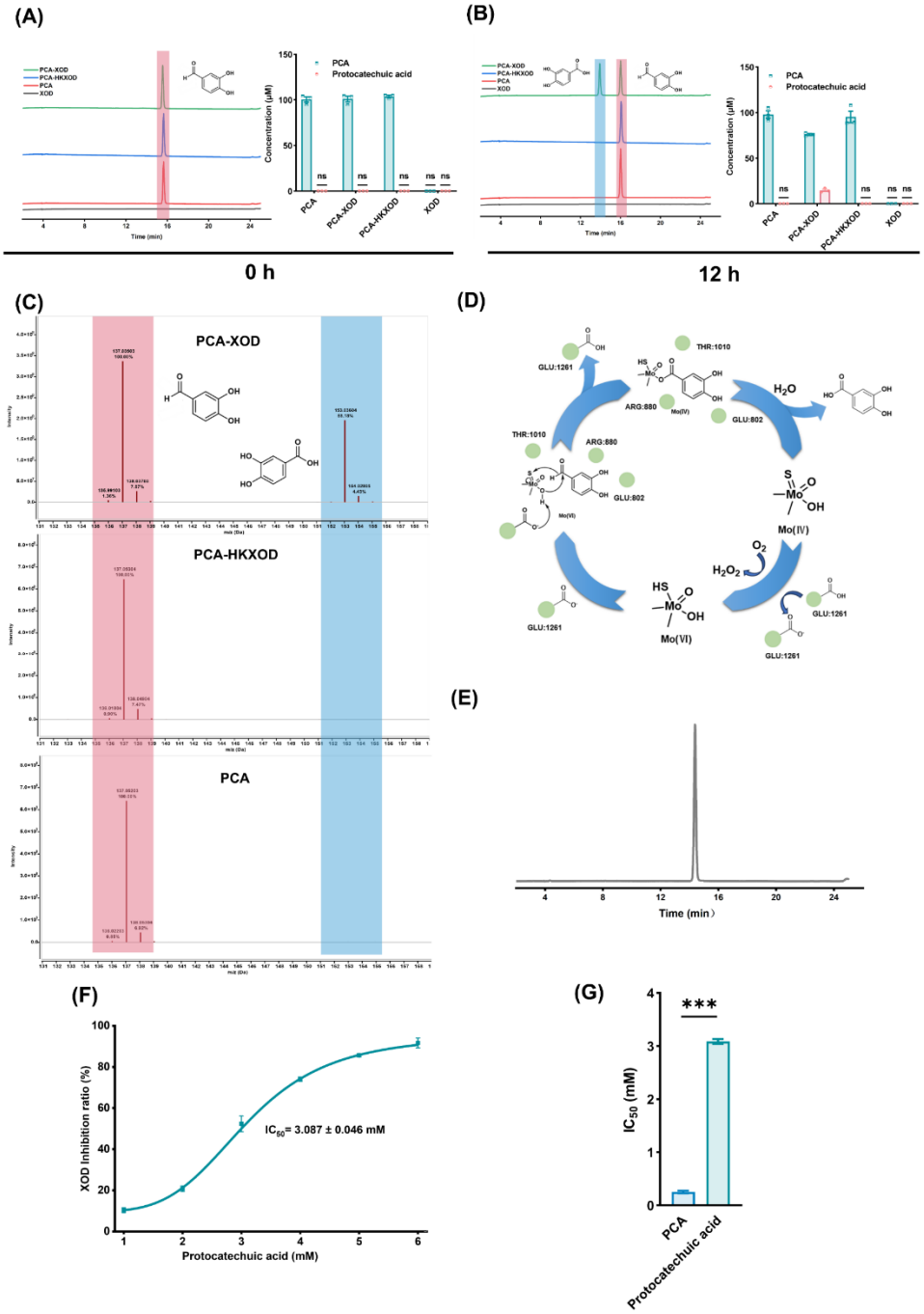

Figure 9. PCA directly targets XOD by functioning as a competitive substrate (A) The HLPC fingerprint pattern of PCA-XOD, PCA-HKXOD, PCA and XOD system at 0 h and (B) 12 h; (C) Mass of PCA-XOD, PCA-HKXOD, and PCA system; (D) Potential mechanism of catalytic cycle; (E) The HLPC fingerprint pattern of protocatechuic acid -XOD; (F) IC_{50} value of protocatechuic acid; (G) IC_{50} value of [PCA] vs [protocatechuic acid]. "ns" indicates that no detection was made.

4. Discussion

The prevalence of HUA continues to rise and is increasingly affecting younger populations, posing a global public health challenge [1]. Current first-line treatments (AP and febuxostat) carry significant safety concerns. Furthermore, treatment strategies for asymptomatic cases remain controversial [5]. Currently, plant-derived compounds, including phenolic acids, flavonoids, and terpenoids, are being investigated for their potential to alleviate HUA [40]. TO, a traditional edible plant, is rich in phenolic acids and flavonoids [14]. Consequently, it holds promise as a dietary supplement for managing HUA.

XOD serves as the key rate-limiting enzyme in UA biosynthesis, with its activity directly modulating UA production. PCA was a strong XOD inhibitor isolated from TO (IC_{50}=0.250 mM). That surpassing established natural XOD inhibitors, such as caffeic acid, luteolin, apigenin, and p-coumaric acid. Furthermore, the practical application of flavonoids (such as luteolin and apigenin) is severely hindered by limited aqueous solubility and low oral bioavailability [41]. In contrast, PCA, as a low-molecular-weight phenolic aldehyde, possesses favorable physicochemical properties, which confers significant pharmacokinetic advantages. Specifically, the absolute oral bioavailability of luteolin and apigenin is extremely low, at only 4.10% and 0.71% [41], respectively. Conversely, protocatechuic aldehyde is extremely rapidly absorbed by the gastrointestinal tract following oral administration (T_{max}=0.17 h) [42]. Its absolute bioavailability reaches 41.79% [42], which was approximately 10-fold and 60-fold higher than that of luteolin and apigenin, respectively. Taken together, PCA is a structurally simple yet highly potent natural XOD inhibitor.

Understanding the mechanistic basis of enzyme inhibition is crucial for evaluating the therapeutic potential of inhibitors. PCA acted as a reversible mixed-type inhibitor, with competitive inhibition playing a dominant role. This inhibition pattern was similar to that reported for phenolic XOD inhibitors, such as p-coumaraldehyde and p-benzaldehyde [12]. However, we have revealed that PCA uniquely functions as a "slow-turnover substrate" through the aldehyde group at the C-1 position, rather than a traditional passive competitive inhibitor. PCA binds to XOD via a strongly exothermic reaction (ΔH=−16.67 Kcal/M) with remarkably high affinity (K_m =14 uM). Crucially, while PCA shares a comparable with the natural substrate xanthine (K_m=12.9 uM [43]), its catalytic turnover is extraordinarily low (K_{cat}=0.014 s^{-1}, compared to 18.31 s^{-1} of xanthine [44]). The combination of high-affinity binding and extremely slow conversion created a kinetic trap. XOD catalysis requires appropriate conformational flexibility of the active pocket to support proton transfer, intermediate and transition-state stabilization, hydride transfer, and water-channel participation [44,45]. The extremely low K_{cat} of PCA might arise from its stable anchoring within the active site. This binding mode induced a more compact and less flexible catalytic pocket, as indicated by lower Rg, SASA, and catalytic-region RMSF. Such restricted dynamics may limit the conformational adjustments required for XOD catalytic turnover. As a result, XOD tied up in PCA processing for a long period and thus continuously blocking xanthine oxidation. Meanwhile, this process causes XOD to adopt a compact and rigid conformation, blocking the substrate channel. In summary, PCA exerts its potent inhibitory effect on XOD through the pathway of “high-affinity anchoring, slow enzymatic consumption, and conformational change. It is worth

noting that, compared to other natural compounds, the mechanism by which PCA blocks UA production was conceptually highly similar to the inhibition strategy of AP [10]. However, allopurinol is catalytically oxidized by XOD to oxprenolol, and its reactive intermediates are associated with life-threatening hypersensitivity reactions. In contrast, the product of PCA was protocatechuic acid. It is safe and possesses multiple bioactive functions. This renders PCA a unique XOD inhibitor that combines inhibition with beneficial transformation, distinct from previously reported natural and clinical XOD inhibitors.

Translating *in vitro* potency into *in vivo* efficacy was a critical step in validating a candidate compound. *In vivo* studies have confirmed that PCA effectively reduced UA production by inhibiting XOD activity. Furthermore, the liver is the main organ for uric acid synthesis [5,46]. After PCA intervention, the XOD expression level in the liver decreased, which was consistent with that of natural products such as ellagic acid, apigenin 7-O-glucoside, and α-viniferin [47-49]. Persistent elevation of UA level can lead to a disruption of the balance between oxidative stress-inflammatory homeostasis in the body. Further damaging the function and structure of the kidney, inducing kidney fibrosis [49-52]. PCA intervention reshapes the renal oxidative stress-inflammation microenvironment and promotes the recovery of renal function and structure. In addition to the reduction of UA level, the anti-inflammatory and antioxidant activities of PCA may also synergistically contribute to this effect. It has been demonstrated that PCA attenuates renal oxidative stress through activation of the Nrf2/SOD pathway and suppresses the expression of inflammatory mediators [53,54].

5. Conclusion

Our work identified PCA as a unique class of natural XOD inhibitor whose inhibitory mechanism was achieved by acting as a competitive substrate. As a slow-turnover substrate, PCA exploits the enzyme’s own catalytic cycle to form a kinetic trap, thereby achieving potent and sustained inhibition of XOD. It was worth noting that the "acting as a competitive substrate" mechanism provides a new reference for the design and screening of mechanism-based XOD inhibitors. Furthermore, the work also provided strong scientific evidence for using TO as a safe and effective dietary supplement or dietary intervention for HUA to address the public health challenges posed by HUA.

Declaration of Interest Statement

The authors declare no competing interest.

Acknowledgments

This work was supported by the National Natural Science Foundation of China under Grant numbers 22238001, 32300794, and 32271488; the National Key Research and Development Program of China (2024YFC0918000); the Beijing Nova Program (20250484890); and the Fundamental Research Funds for the Central Universities (BUCT-ZR-2601).

References

[1]. L. Du; Y. Zong; H. Li, et al. Hyperuricemia and its related diseases: mechanisms and advances in therapy. *Signal Transduction and Targeted Therapy. 9* (2024). 10.1038/s41392-024-01916-y.

[2]. N. Dalbeth; T. R. Merriman; L. K. Stamp. Gout. *Lancet. 388* (2016) 2039–2052. 10.1016/S0140-6736(16)00346-9.

[3]. N. Kumar; K. Kaur; N. Kaur, et al. Pathology, target discovery, and the evolution of XO inhibitors from the first discovery to recent advances (2020–2023). *Bioorganic Chemistry. 143* (2024). 10.1016/j.bioorg.2023.107042.

[4]. Y. Zhao; R. Wang; R. Cao, et al. Galangin Protects against Hyperuricemia via Ameliorating Gut-Kidney Axis Dysfunction in Mice. *J Agric Food Chem. 73* (2025) 13902–13917. 10.1021/acs.jafc.5c01260.

[5]. J. Guo; H. Liu; T. Jin, et al. Moslae Herba extract alleviates hyperuricemia by regulating uric acid metabolism and relieving renal inflammation and fibrosis in mice. *Phytomedicine. 145* (2025) 156974. 10.1016/j.phymed.2025.156974.

[6]. W. Zeng; M. Ghamry; Z. Zhao, et al. Hyperuricemia insights: Formation, targets and hypouricemic natural products. *Food Bioscience. 64* (2025). 10.1016/j.fbio.2025.105944.

[7]. H. Xia; W. He; C. Lv, et al. The inhibitory effect of Astragalus flavone extract on hyperuricemia and its underlying molecular mechanism by targeting JNK/AP-1/NLRP3/IL-1beta signaling pathway. *Phytomedicine. 140* (2025) 156622. 10.1016/j.phymed.2025.156622.

[8]. G. Wu; H. Dong; T. Li, et al. Dietary Oligosaccharides Isolated from Coix Seed Mitigate Hyperuricemia through Modulation of Lipid Metabolites and Intestinal Homeostasis. *J Agric Food Chem. 73* (2025) 4078–4093. 10.1021/acs.jafc.4c09397.

[9]. S. Yang; Q. Chen; Y. You, et al. Molecular mechanisms of Lycii Fructus (Goji berries) against xanthine dehydrogenase in hyperuricemia management: Integrating computational, metabolomic, and experimental approaches. *Food Res Int. 204* (2025) 115926. 10.1016/j.foodres.2025.115926.

[10]. P. Pacher; A. Nivorozhkin; C. Szabo. Therapeutic effects of xanthine oxidase inhibitors: renaissance half a century after the discovery of allopurinol. *Pharmacol Rev. 58* (2006) 87–114. 10.1124/pr.58.1.6.

[11]. T. M. Ngoc; N. M. Khoi; D. T. Ha, et al. Xanthine oxidase inhibitory activity of constituents of Cinnamomum cassia twigs. *Bioorganic & Medicinal Chemistry Letters. 22* (2012) 4625–4628. 10.1016/j.bmcl.2012.05.051.

[12]. X. Wang; B. Chen; S. Wu, et al. Inhibition of xanthine oxidase by two aldehydes: Inhibitory kinetics, molecular simulation, inhibition mechanism, and cellular insights. *Int J Biol Macromol. 330* (2025) 148050. 10.1016/j.ijbiomac.2025.148050.

[13]. M. Martinez; P. Poirrier; R. Chamy, et al. Taraxacum officinale and related species-An ethnopharmacological review and its potential as a commercial medicinal plant. *J Ethnopharmacol. 169* (2015) 244–262. 10.1016/j.jep.2015.03.067.

[14]. B. Lis; B. Olas. Pro-health activity of dandelion (Taraxacum officinale L.) and its food products – history and present. *Journal of Functional Foods. 59* (2019) 40–48. 10.1016/j.jff.2019.05.012.

[15]. D. Jedrejek; S. Pawelec. Comprehensive Qualitative and Quantitative Analysis of Flavonoids in Dandelion (Taraxacum officinale) Flowers and Food Products. *J Agric Food Chem. 72* (2024) 17368–17376. 10.1021/acs.jafc.4c03108.

[16]. J. Yao; Z. Ma; Y. Wang, et al. Effects of dandelion addition on antioxidant property, sensory characteristics and inhibitory activity against xanthine oxidase of beer. *Current Research in Food Science. 5* (2022) 927–939. 10.1016/j.crfs.2022.05.008.

[17]. A. Karakuş; Y. Değer; S. Yıldırım. Protective effect of Silybum marianum and Taraxacum officinale extracts against oxidative kidney injuries induced by carbon tetrachloride in rats. *Renal Failure. 39* (2017) 1–6. 10.1080/0886022X.2016.1244070.

[18]. Q. Hu; J. Ji; D. Xu, et al. Isolation and characterization of uric acid-lowering functional components from Polygonum cuspidatum. *Food Bioscience. 53* (2023). 10.1016/j.fbio.2022.102314.

[19]. S. Wen; D. Wang; H. Yu, et al. The Time-Feature of Uric Acid Excretion in Hyperuricemia Mice Induced by Potassium Oxonate and Adenine. *International Journal of Molecular Sciences. 21* (2020). 10.3390/ijms21155178.

[20]. Q. Yang; S. Su; N. Luo, et al. Adenine-induced animal model of chronic kidney disease: current applications and future perspectives. *Renal Failure. 46* (2024). 10.1080/0886022x.2024.2336128.

[21]. S. Han; Z. Wang; J. Liu, et al. miR-29a-3p-dependent COL3A1 and COL5A1 expression reduction assists sulforaphane to inhibit gastric cancer progression. *Biochemical Pharmacology. 188* (2021). 10.1016/j.bcp.2021.114539.

[22]. X. Liu; W. Zhang; J. Chen, et al. Investigating the inhibition of xanthine oxidase by five catechins: Kinetic studies, spectroscopy, molecular docking, and dynamics simulations. *Int J Biol Macromol. 281* (2024) 136231. 10.1016/j.ijbiomac.2024.136231.

[23]. Y. Yao; A. Ma; Q. Huang, et al. The novel mechanism on the inhibition of superoxide anion generating from xanthine oxidase in the presence of myricetin. *International Journal of Biological Macromolecules. 283* (2024). 10.1016/j.ijbiomac.2024.137636.

[24]. B. Zambelli. Characterization of Enzymatic Reactions Using ITC. In *Microcalorimetry of Biological Molecules*; Methods in Molecular Biology; 2019; pp. 251–266.

[25]. Z. Yu; Y. Cao; R. Kan, et al. Identification of egg protein-derived peptides as xanthine oxidase inhibitors: virtual hydrolysis, molecular docking, and in vitro activity evaluation. *Food Science and Human Wellness. 11* (2022) 1591–1597. 10.1016/j.fshw.2022.06.017.

[26]. M. Tian; P. Yu; Z. Li, et al. Effects and mechanism of metal ions on the stability of glucosinolates in aqueous solution. *Food Chemistry. 448* (2024). 10.1016/j.foodchem.2024.139098.

[27]. K. Li; Y. Wang; W. Liu, et al. Structure-Activity Relationships and Changes in the Inhibition of Xanthine Oxidase by Polyphenols: A Review. *Foods. 13* (2024). 10.3390/foods13152365.

[28]. J. Yan; G. Zhang; Y. Hu, et al. Effect of luteolin on xanthine oxidase: inhibition kinetics and interaction mechanism merging with docking simulation. *Food Chem. 141* (2013) 3766–3773. 10.1016/j.foodchem.2013.06.092.

[29]. X. Liu; J. Dong; J. Cui, et al. Microalgae-based drug delivery microspheres for treatment of hyperuricemia with renal injury. *Nano Today. 61* (2025). 10.1016/j.nantod.2024.102607.

[30]. Y. Wang; W. Kong; L. Wang, et al. Multiple-Purpose Connectivity Map Analysis Reveals the Benefits of Esculetin to Hyperuricemia and Renal Fibrosis. *Int J Mol Sci. 21* (2020). 10.3390/ijms21207695.

[31]. J. Sun; Z. Shen; Y. Sun, et al. Comparison of the anti-hyperuricemia effects of several cinnamic acid derivatives. *J Sci Food Agric. 105* (2025) 6341–6347. 10.1002/jsfa.14341.

[32]. E. R. DeVallance; H. M. Schmidt; M. Seman, et al. Hemin and iron increase synthesis and trigger export of xanthine oxidoreductase from hepatocytes to the circulation. *Redox Biol. 67* (2023) 102866. 10.1016/j.redox.2023.102866.

[33]. W. K. Han; V. Bailly; R. Abichandani, et al. Kidney Injury Molecule-1 (KIM-1): a novel biomarker for human renal proximal tubule injury. *Kidney Int. 62* (2002) 237–244. 10.1046/j.1523-1755.2002.00433.x.

[34]. J. Li; Y. Gong; J. Li, et al. In vitro inhibitory effects of polyphenols from Tartary buckwheat on xanthine oxidase: Identification, inhibitory activity, and action mechanism. *Food Chem. 379* (2022) 132100. 10.1016/j.foodchem.2022.132100.

[35]. Y. Lou; Q. Gao; M. Fan, et al. Ferulic acid ameliorates hyperuricemia by regulating xanthine oxidase. *Int J Biol Macromol. 253* (2023) 126542. 10.1016/j.ijbiomac.2023.126542.

[36]. Y. Yao; M. Zhang; J. Chen, et al. Novel mechanistic insights into Luteolin and its analogues as potent inhibitors of xanthine oxidase activity: Inhibition thermodynamics, kinetics and docking simulation. *Food Bioscience. 71* (2025). 10.1016/j.fbio.2025.107087.

[37]. S. M. Buker; P. A. Boriack-Sjodin; R. A. Copeland. Enzyme-Inhibitor Interactions and a Simple, Rapid Method for Determining Inhibition Modality. *SLAS Discov. 24* (2019) 515–522. 10.1177/2472555219829898.

[38]. R. A. Copeland. *Reversible Modes of Inhibitor Interactions with Enzymes*; Wiley.: 2013; pp. 57–121.

[39]. Y. Du; Z. Liu; F. Qiao, et al. Computational exploration of reactive fragment for mechanism-based inhibition of xanthine oxidase. *Journal of Organometallic Chemistry. 864* (2018) 58–67. 10.1016/j.jorganchem.2018.01.018.

[40]. S. Feng; S. Wu; F. Xie, et al. Natural compounds lower uric acid levels and hyperuricemia: Molecular mechanisms and prospective. *Trends in Food Science & Technology. 123* (2022) 87–102. 10.1016/j.tifs.2022.03.002.

[41]. S. Wu; S.-T. Wang; G.-Y. Chen, et al. Monophosphate Derivatives of Luteolin and Apigenin as Efficient Precursors with Improved Oral Bioavailability in Rats. *Antioxidants. 13* (2024). 10.3390/antiox13121530.

[42]. X. Wang; K. Yan; X. Ma, et al. Simultaneous Determination and Pharmacokinetic Study of Protocatechuic Aldehyde and Its Major Active Metabolite Protocatechuic Acid in Rat Plasma by Liquid Chromatography-Tandem Mass Spectrometry. *J Chromatogr Sci. 54* (2016) 697–705. 10.1093/chromsci/bmv240.

[43]. M. Mangino; J. Brunner. Isolation and partial characterization of xanthine oxidase associated with the milk fat globule membrane of cows' milk. *Journal of Dairy Science. 60* (1977) 841–850.

[44]. P. M. G. Ribeiro; H. S. Fernandes; L. B. Maia, et al. The complete catalytic mechanism of xanthine oxidase: a computational study. *Inorganic Chemistry Frontiers. 8* (2021) 405–416. 10.1039/d0qi01029d.

[45]. S. Metz; W. Thiel. A Combined QM/MM Study on the Reductive Half-Reaction of Xanthine Oxidase: Substrate Orientation and Mechanism. *Journal of the American Chemical Society. 131* (2009) 14885–14902. 10.1021/ja9045394.

[46]. W. G. Lima; M. E. Martins-Santos; V. E. Chaves. Uric acid as a modulator of glucose and lipid metabolism. *Biochimie. 116* (2015) 17–23. 10.1016/j.biochi.2015.06.025.

[47]. X. L. Guo; Y. Y. Gao; Y. X. Yang, et al. Amelioration effects of alpha-viniferin on hyperuricemia and hyperuricemia-induced kidney injury in mice. *Phytomedicine. 116* (2023) 154868. 10.1016/j.phymed.2023.154868.

[48]. Y. Zhang; Y. Li; C. Li, et al. Paeonia x suffruticosa Andrews leaf extract and its main component apigenin 7-O-glucoside ameliorate hyperuricemia by inhibiting xanthine oxidase activity and regulating renal urate transporters. *Phytomedicine. 118* (2023) 154957. 10.1016/j.phymed.2023.154957.

[49]. Z. R. Sun; H. R. Liu; D. Hu, et al. Ellagic Acid Exerts Beneficial Effects on Hyperuricemia by Inhibiting Xanthine Oxidase and NLRP3 Inflammasome Activation. *J Agric Food Chem. 69* (2021) 12741–12752. 10.1021/acs.jafc.1c05239.

[50]. N. Liu; H. Xu; Q. Sun, et al. The Role of Oxidative Stress in Hyperuricemia and Xanthine Oxidoreductase (XOR) Inhibitors. *Oxid Med Cell Longev. 2021* (2021) 1470380. 10.1155/2021/1470380.

[51]. Y. Wang; H. Jiang; L. Zhang, et al. Nanosystems for oxidative stress regulation in the anti-inflammatory therapy of acute kidney injury. *Front Bioeng Biotechnol. 11* (2023) 1120148. 10.3389/fbioe.2023.1120148.

[52]. R. Huang; P. Fu; L. Ma. Kidney fibrosis: from mechanisms to therapeutic medicines. *Signal Transduction and Targeted Therapy. 8* (2023). 10.1038/s41392-023-01379-7.

[53]. I. Mssillou; Y. El Abdali; F. E. Amrati, et al. Unlocking the therapeutic potential of protocatechualdehyde: pharmacological applications and mechanism insights. *Naunyn Schmiedebergs Arch Pharmacol. 398* (2025) 15113–15139. 10.1007/s00210-025-04267-9.

[54]. Z. S. Tao; X. F. Hu; X. J. Wu, et al. Protocatechualdehyde inhibits iron overload-induced bone loss by inhibiting inflammation and oxidative stress in senile rats. *Int Immunopharmacol. 141* (2024) 113016. 10.1016/j.intimp.2024.113016.